Wellman, S. A., A. Olivo, I. T. Gloppen, and H. Teisrud. 2026. Improved slag estimation in metallurgical grade silicon via temperature-resolved analysis. In *Silicon for the Chemical and Solar Industry XVIII*, edited by M. Tangstad, H. Rong, A. Valderhaug, B. Andresen, H. Dalaker, and I. G. Page. Kristiansand, Norway, September 7–10. https://doi.org/10.55669/oa900827

# Improved slag estimation in metallurgical grade silicon *via* temperature-resolved analysis

**S.A. Wellman[1,2], A. Olivo[2], I.T. Gloppen[2], and H. Teisrud[2]**
[1]Norwegian University of Science and Technology (NTNU), Dept. of Physics, Trondheim, Norway (sophiaaw@stud.ntnu.no)
[2]Elkem ASA, Kristiansand, Norway (alberto.olivo@elkem.com, ida-therese.gloppen@elkem.com, hege.teisrud@elkem.com)

*Keywords:* slag estimation, silicon production, quality control, oxygen measurements, inert gas fusion

**Abstract –** Accurate quantification of slag in silicon is essential for quality control in industrial silicon production. Conventional combustion methods provide only total oxygen content and cannot distinguish between slag-derived oxygen and that originating from surface oxides, leading to variability influenced by particle size and sample preparation. This study presents a modified analytical approach based on controlled temperature ramping to selectively differentiate oxygen contributions from surface silicon oxides ($SiO_x$) and slag phases. The method exploits thermodynamic differences between oxygen containing species, enabling their separation through temperature resolved evolution profiles. Systematic method development was carried out on silicon materials with varying purity, including metallurgical grade (MG-Si) and electronic grade silicon (EG-Si). The results demonstrate that slag-related oxygen is released at higher temperatures than surface oxides, allowing clear signal separation. The proposed method shows strong potential for improving slag estimation accuracy and providing more robust oxygen speciation in silicon quality assessment.

## 1. INTRODUCTION

Elkem produces a wide range of silicon-based materials, including ferrosilicon (FeSi), magnesium ferrosilicon (FSM), and silicon powders of varying purities, for all of which slag content represents a critical quality parameter (Elkem ASA, n.d.). Quantification of slag is performed using oxygen content as a proxy (Johnston and Barati, 2010). Therefore, the validity of the slag content estimation relies on the reliability of the oxygen measurements. Quantification of slag in silicon materials must be accurate and reproducible to ensure reliable quality control in industrial silicon production (Næss *et al.*, 2014).

In general, the oxygen measurements from which slag content is inferred are obtained by inert gas fusion (IGF) analysis. The standard IGF procedure provides only a total oxygen value and does not distinguish between oxygen originating from slag and oxygen associated with $SiO_x$ (Maslennikova *et al.*, 2025).

To obtain representative results and thus reduce variability, sample homogeneity is crucial: to this purpose, silicon is crushed to micron-range powder prior to analysis. Crushing is a necessary step in samples preparation for IGF and it allows for better mixing of the slag in the silicon (Gruner and John, 1992), even though the material is likely to separate into a heterogeneous mixture where finer particles reside closer to the surface. Crushing and milling increase the surface-to-volume ratio of the sample, thereby enhancing the contribution from surface oxides and introducing errors in the estimated slag content (Petrakis and Komnitsas,

2022). Generally, crushing is operator-dependent since it is affected by several parameters, such as different equipment type, feed rate, and milling time (Nilssen and Kleiv, 2019). Consequently, particle size distributions vary between specimens and sites so that samples that were crushed for longer or milled finer will suffer to a larger extent from increased oxygen contribution from the surface silicon oxide (Kim *et al.*, 2011). Therefore, measurement errors are both systematic and random in nature: systematic due to the direct correlation of increased surface oxygen with decreasing particle size, and random due to variability in operational conditions (Shen *et al.*, 1997). This challenge is widely recognised within the silicon industry, but available open literature on analytical methods remains limited (Forwald *et al.*, 1994). To the author's knowledge, there is only a patent by Miller, but its applicability is limited to Si powders whose size is suitable for further processing in organohalosilane industry (< 150 μm; Kuivila and Miller, 1999). Furthermore, the patent does not report the extent to which the proposed method improves measurement precision, limiting the assessment of its analytical performance.

Currently, the contribution of $SiO_x$ is not deducted from the total oxygen content when estimating slag content, resulting in the incorrect classification of MG-Si production batches as *off-specification* and subsequently in unnecessary rework. Consequently, there is a need for an analytical approach that can discriminate between oxygen contributions from surface $SiO_x$ and slag phases.
This study investigates a modified analytical method designed to this purpose through a controlled temperature-ramping programme. The approach exploits thermodynamic differences in decomposition reactions among oxygen-containing phases, causing their reactions to occur at distinct temperature intervals (Ostrovski *et al.*, 2010). To the authors' knowledge, no previous studies have reported the use of temperature-resolved inert gas fusion analysis to quantitatively differentiate oxygen associated with surface $SiO_x$ from oxygen originating from slag phases in metallurgical-grade silicon (MG-Si).

A sequence of method iterations was evaluated on silicon samples of varying purity, including metallurgical-grade silicon (MG-Si) and electronic-grade silicon (EG-Si) to confirm that slag-related oxygen evolves at higher temperatures than surface oxides, thereby enabling separation of the two signals. Moreover, an additive was tested to accelerate $SiO_x$ decomposition without affecting slag, thus improving signal resolution.
The method is finally verified through a controlled milling experiment using MG-Si (99 wt. % Si), where increasing milling time, and thus surface area, is expected to increase the oxygen signal associated with $SiO_x$,while leaving slag-related signal statistically unchanged. The results serve as proof-of-concept for a selective temperature-programmed method capable of separating surface oxide and slag contributions to the total oxygen content.

The approach has the potential to reduce misclassification of silicon batches caused by surface-oxide artefacts, improve analytical robustness across production sites, and strengthen quality-control procedures in silicon manufacturing.

## 2. EXPERIMENTAL

### 2.1 Materials

A MG-Si reference sample was used as a model material for initial proof-of-concept testing. It contains more than 99 wt. % elemental Si and the main metal impurities are Fe (0.35 wt. %), Al (0.12 wt. %), C (0.011 wt. %), Ca (350 ppm), and Ti (250 ppm) (Elkem ASA, 2024). Before IGF testing, MG-Si was pulverised in a laboratory planetary mill until $D_{50}$ was lower than 20 μm.

During IGF analysis, oxygen originating both from slag phases and from surface oxides is detected. To verify the assignment of oxygen signals to specific oxygen-containing species in Si-99, the signal profiles of Silgrain® e-Si as a reference EG-Si (purity > 99.9 wt. %, $D_{50}$=1.50 μm) and wollastonite ($Ca_3(Si_3O_9)$), as a representative pure slag material, were studied. The former has minimal amounts of slag due to its high purity such that the oxygen detected for this material is expected to be mainly from $SiO_x$. This powder will therefore allow the identification of $SiO_x$ signal assignment in MG-Si. On the contrary, wollastonite was chosen due to its simple chemical composition, absence of free elemental Si, and relevance to silicon metallurgy (Jiang *et al.*, 2014). The tests with wollastonite will then ascribe the signal placement to slag unambiguously.

**2.2 Inert gas fusion analysis**

For this study, IGF was carried out using a dedicated commercial instrument, LECO ON 836, (LECO, n.d.). Since the instrument operates in inert conditions, leak check and blank correction test are run before each measurements session. For improved homogenisation, the bulk of the sample is first manually mixed prior to the sampling. Before each measurement, approximately a 0.2 g specimen is weighed using tin foil as a container. The foil is subsequently folded and then introduced into a graphite crucible containing graphite powder for IGF in the furnace under helium flow.

Some experiments make use of nickel as a flux medium. The additive was used, as recommended by the instrument supplier, to enhance the reaction kinetics of oxide phases during IGF analysis. For these tests, the sample was placed in a nickel basket before the assembly was introduced to the graphite crucible.

In the analysis, inorganic oxides undergo carbothermic reaction, which is followed by the Boudouard reaction (Eq. [1] and [2]). Added graphite will then act as a reductant for $M_xO_y$ species.

$$M_xO_y + yC \rightarrow yCO + xM \quad [1]$$

$$2CO \rightarrow CO_2 + C \quad [2]$$

where $M_xO_y$ is a general formula for oxide and M its elemental form. Therefore, oxygen signal is calculated *via* the quantification of CO and $CO_2$, which are detected using a non-dispersive infrared (NDIR) cell. The oxygen concentration is derived using the principle that analyte gas molecules absorb infrared (IR) energy at unique wavelengths and there is a correlation between concentration and IR absorbance (LECO, n.d.). The oxygen signal was recorded as a function of time and furnace temperature and subsequently normalised to sample mass for comparison between measurements. As the aim was to compare relative oxygen-release profiles rather than determine absolute oxygen concentrations, no calibration was applied; the raw detector signal was instead used directly and normalised to sample mass (Skoog *et al.*, 2017). The number of replicates was selected based on the need to ensure sufficient precision and to capture method variability, in line with established principles of analytical chemistry (Skoog *et al.*, 2017). In this study, two to three replicates were applied during exploratory experiments to obtain an initial indication of repeatability. For experiments requiring a more robust statistical evaluation, the number of replicates was increased to five or more, particularly to account for variability associated with sample inhomogeneity.

**2.3 Temperature-ramping programme**

The oxygen-containing species present in MG-Si include adsorbed water, carbonates, surface silicon oxides, and slag phases. Adsorbed water and carbonates are expected to decompose at

relatively low temperatures (up to approximately 900 °C). Silicon oxides are anticipated to be reduced at intermediate temperatures between 1600 °C and 1700 °C (Lee *et al.*, 2010), whereas slag-related oxygen species are reduced at higher temperatures (above 2200 °C). Accordingly, the temperature ramping programme was designed as a sequence of discrete temperature intervals. Each interval was selected to be sufficiently high to promote decomposition of a specific oxygen-containing species, while minimising overlap with subsequent reactions. The expected sequence of decomposition is illustrated in Figure 1.

The temperature programme was iteratively refined during the experimental campaign to maximise the separation between $SiO_x$ decomposition and the onset of slag reduction. Adjustments included extending the dwell time at the $SiO_x$ decomposition plateau and introducing nickel as a flux to facilitate the reduction of silicon oxides. Efforts were additionally made to improve the signal resolution between the $SiO_x$ and slag-related oxygen signals. To facilitate the interpretation of the oxygen-evolution profiles, the corresponding temperature programme is shown on the secondary y-axis in all plots presented in Chapter 3.

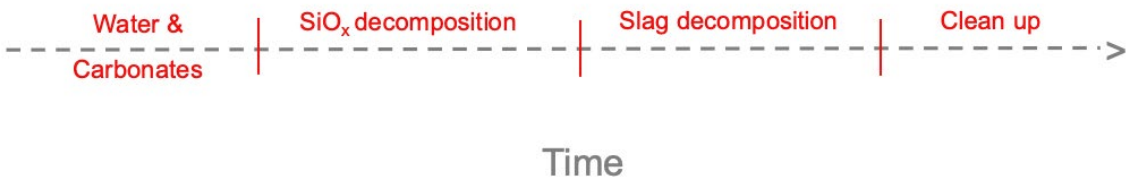


**Figure 1:** Schematic representation of oxygen-containing species decomposition during temperature ramping

**2.4 Proof of concept experiment**

To verify the method, a proof-of-concept experiment was conducted using Si-99 samples subjected to varying milling durations, thereby producing different particle size distributions. Increased milling time results in reduced particle size and, consequently, a higher surface-area to-volume ratio, leading to increased surface oxide content. It is therefore expected that the signal corresponding to the $SiO_x$ decomposition interval increases with milling duration, while the signal associated with slag decomposition remains largely unaffected.

For this experiment, as-received MG-Si was milled in a *PULVERISETTE 7 premium line* planetary mill from Fritsch. at 1100 rpm spinning rate for 10 s, 30 s, and 60 s. Specific surface area (SSA) was determined by nitrogen physisorption using a Micromeritics TriStar analyser. Prior to measurement, the samples were degassed to remove adsorbed moisture and volatile species, and the surface area was calculated from the adsorption isotherm in the $p/p_0$ =0.05-0.30 range using the BET method (Brunauer *et al.*, 1938).
An unmilled sample was also analysed, resulting in four MG-Si samples with distinct particle size distributions and surface oxide contents. Sample preparation otherwise followed the procedure described in Section 2.1 where five replicates were prepared from each sample batch. When needed, pairwise two-sample t-tests were used to assess whether differences in integrated peak areas were statistically significant; $p < 0.01$ was taken as the significance threshold.

## 3. RESULTS AND DISCUSSION

The carbothermic reduction is generally defined as the chemical reactions that occur between metal oxides and elemental carbon to form carbon monoxide and (semi)metals in their elemental form (see Eq. [1]). These are the same type of reactions that occur in a silicon furnace, therefore similar considerations can be used to describe MG-Si production and oxygen quantification *via* IGF.

The minimum temperature required for carbothermic reduction is defined thermodynamically as the temperature at which the Gibbs free energy of the overall reduction reaction becomes zero ($\Delta G = 0$), corresponding to equilibrium between oxide, carbon, and gaseous species (L'vov, 2000). In this condition, the oxygen affinity to carbon equals that to the oxide, and reduction becomes feasible at higher temperatures (Chahtou *et al.*, 2020). In practical systems, this temperature is not fixed but depends on gas composition, pressure, and reactant activities, which determines the onset of carbothermic reduction in the IGF furnace.
The reaction mechanism is applicable to many elements, such as aluminium, silicon, titanium, iron, etc. (Ostrovski *et al.*, 2010). During the analysis, when a high enough temperature is reached, metal oxides in the sample (i.e. $SiO_x$ and wollastonite) react *via* carbothermic reduction mechanisms with the graphite powder in the crucible.

In the case of $SiO_2$, this reaction occurs at temperatures higher than 1600 °C (Maeng *et al.*, 2020). The oxidation product, i.e. CO, is then disproportionated to $CO_2$ and elemental C in the Boudouard reaction (see Eq. [2]). $SiO_x$ reduction proceeds *via* the formation of gaseous SiO, which then can be further reduced to SiC (see Equations [3] and [4]). This reaction pathway introduces a potential source of analytical uncertainty, since SiO is not directly detected by the NDIR system.

$$SiO_x + (x-1)C \rightarrow SiO + (x-1)CO \quad [3]$$
$$SiO + 2C \rightarrow SiC + CO \quad [4]$$

Thermodynamically, low CO partial pressure favours the further conversion of SiO towards either Si or SiC formation (Schei *et al.*, 1998). Under the present analytical conditions, the continuous helium flow may contribute to maintaining a low local pCO, while the addition of fine graphite increases the available carbon surface area and promotes SiO–carbon contact. These conditions are therefore expected to favour SiO conversion and reduce potential losses, improving the reliability of the oxygen measurement.

Whereas, wollastonite carbothermic reduction occurs at temperatures higher than 2000 °C (Swamy and Dubrovinsky, 1997). Therefore, from a thermodynamic point of view, it is possible to separate signals from $SiO_x$ and wollastonite in a IGF spectrum. However, the fast temperature ramp rate requires the optimisation of analysis parameters to improve robustness of results.

To verify the assignment of signal from $SiO_x$, the temperature-ramping programme was first applied to EG-Si. Its oxygen profile is shown in Figure 2. Two distinct regions of oxygen evolution are present: an early peak at 150-350 s within the designated $SiO_x$ interval (a) and a second peak appearing during the subsequent temperature increase toward the slag plateau (c) at 450-600 s. For EG-Si, the main signal was expected to stay within the designated $SiO_x$ interval. Thus, the resulting splitting of oxygen signal was unexpected. However, upon closer inspection, the onset temperature of the second peak at (c), coincides with that of the $SiO_x$ region (i.e. 1650 °C). Additionally, a sharp decrease in signal is observed upon initiation of the

cooling stage (b) at 350 s, indicating incomplete oxide decomposition in the initial plateau (a). These observations suggest that the second peak represents continued decomposition of residual silicon oxides, temporarily interrupted by the cooling step. This may be attributed to slower reduction kinetics for certain oxide species in $SiO_x$, requiring higher temperatures to overcome activation barriers for carbothermic reduction, or perhaps the $SiO_x$ quantity is too high to be reduced in that short amount of time.

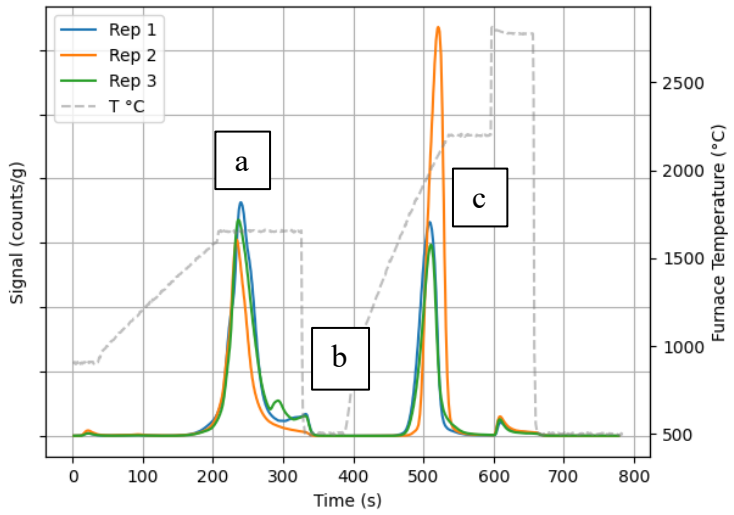


**Figure 2:** Oxygen signal profiles for temperature-ramped combustion of EG-Si without nickel

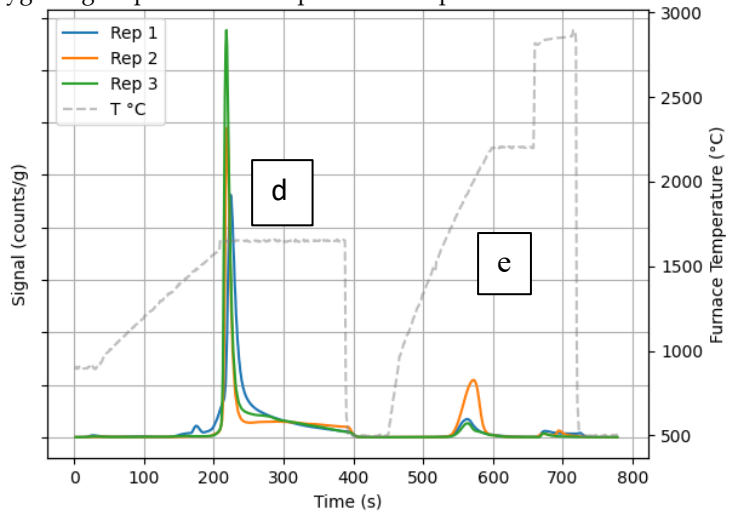


**Figure 3:** Oxygen signal profiles for temperature-ramped combustion of EG-Si with nickel

To improve the kinetics of $SiO_x$ reduction and thus improve the resolution of oxygen measurements with IGF, one can employ nickel, a commonly used flux medium (Beck and Müller, 1997). There are three main reasons for nickel being a commonly chosen flux. Firstly, elemental nickel's melting point is 1455 °C, meaning it is liquid at the $SiO_2$ reduction temperature. In its liquid form, nickel has a higher conductivity than the carrier gas helium (54.6 vs. 0.468 $W \cdot m^{-1} \cdot K^{-1}$ at 1750 °C) and thus enhances heat transfer from furnace heating elements to the specimen (Assael *et al.*, 2017). Secondly, it has been recently proved that Ni has a catalytic effect on $SiO_2$ reduction to Si by weakening bonds in adsorbed CO and SiO and favouring oxygen transfer (Chen *et al.*, 2025). Finally, Ni catalytic effect on CO disproportionation is well-established. The conversion of CO causes a shift in the equilibrium of reaction in Eq. [1], thus boosting metal oxides conversion to their elemental state (Balakos and Chuang, 1993).

As shown in Figure 3, the addition of Ni results in a clear redistribution of the oxygen signal, with a larger fraction occurring within the designated $SiO_x$ interval (d) at 150-300 s. This is evident both qualitatively from peak intensities and quantitatively from peak area analysis (Table I). The fraction of oxygen released at within the designated slag plateau (e) at 450-600 s decreased from 43 % to 9 % upon addition of Ni. These results, summarised in Table I, demonstrate that nickel significantly promotes oxide decomposition at lower temperatures, thereby reducing overlap with the slag-related signal.

**Table I:** Relative oxygen signal contributions in the $SiO_x$ and slag regions, respectively

| Sample | 150-350 s | 450-600 s |
|---|---|---|
| **EG-Si without Ni** | 54.18 % | 42.94 % |
| **EG-Si with Ni** | 88.07 % | 9.25 % |

Identification of the slag-related signal was performed using wollastonite as a model slag material. Experiments were conducted both with and without nickel to assess its influence on slag decomposition kinetics (Figures 4 and 5). The results confirm that slag reduction occurs exclusively in the high-temperature region, well above the $SiO_x$ decomposition interval. Moreover, under selected analytical conditions, the addition of nickel has no observable effect on slag behaviour, suggesting that Ni acts as a selective flux for silicon oxides without influencing slag reduction.

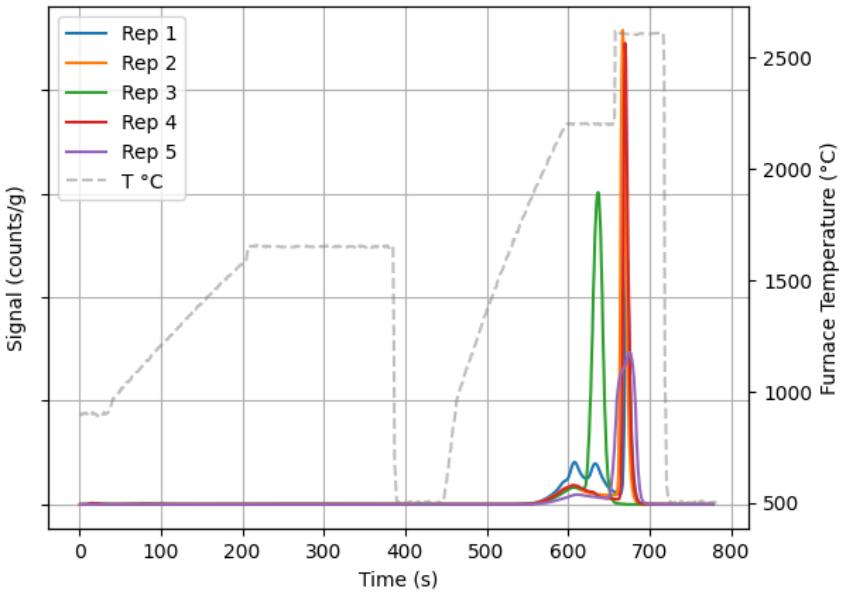


**Figure 4:** Oxygen signal profiles for wollastonite without Ni

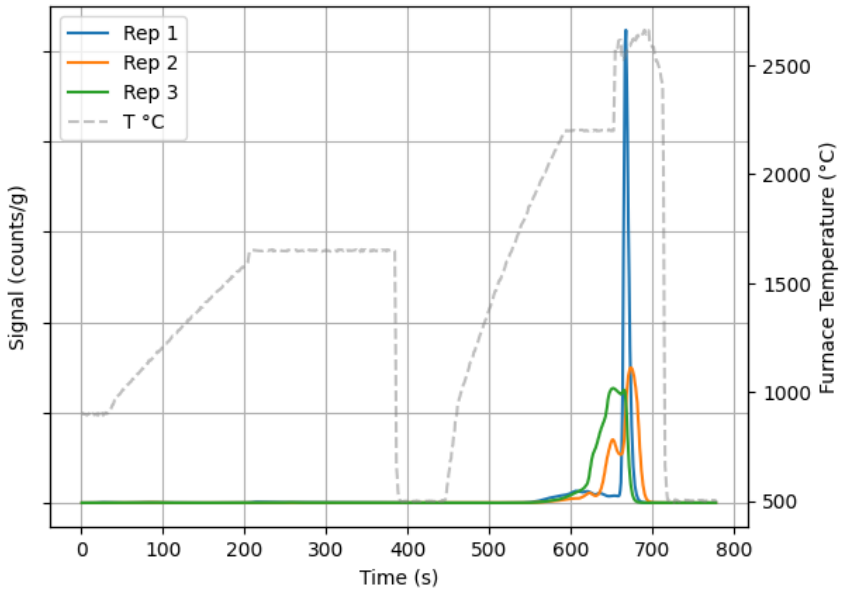


**Figure 5:** Oxygen signal profiles for wollastonite with Ni

Having established signal assignment and confirmed that $SiO_x$ and slag signals could be almost completely separated, the method was evaluated using Si-99 samples subjected to controlled milling for 10, 30, and 60 s. By increasing the milling time, the mean particle size is reduced. This further size reduction caused an increase in SSA from 0.20 $m^2 \cdot g^{-1}$ to 0.51, 1.96, and 3.17 $m^2 \cdot g^{-1}$, respectively. As previously mentioned, a decreased particle size increases the specific surface area, meaning an increased amount of surface silicon oxide is present. The resulting oxygen signal profiles are shown in Figure 6.

A clear increase in signal intensity within the $SiO_x$ region is observed with increasing milling time, consistent with increased surface area and oxide content. The slightly lower onset temperature observed for the coarser particles may be related to differences in oxide accessibility rather than to a true thermodynamic shift in $SiO_x$ reduction. In fact, as milling increases the specific surface area, it may also increase powder bed porosity and create a more tortuous packed structure (Olivo *et al.*, 2024; Watanabe, 2025). This can introduce additional resistance to mass transport towards the $Si/SiO_x$–C reaction interface, delaying the effective release of $CO/CO_2$ from the finer samples. Therefore, the early onset in the coarse sample should be interpreted as a kinetic/sample-heterogeneity effect. In contrast, the signal in the high temperature region remains comparatively stable, both in onset temperature and magnitude.

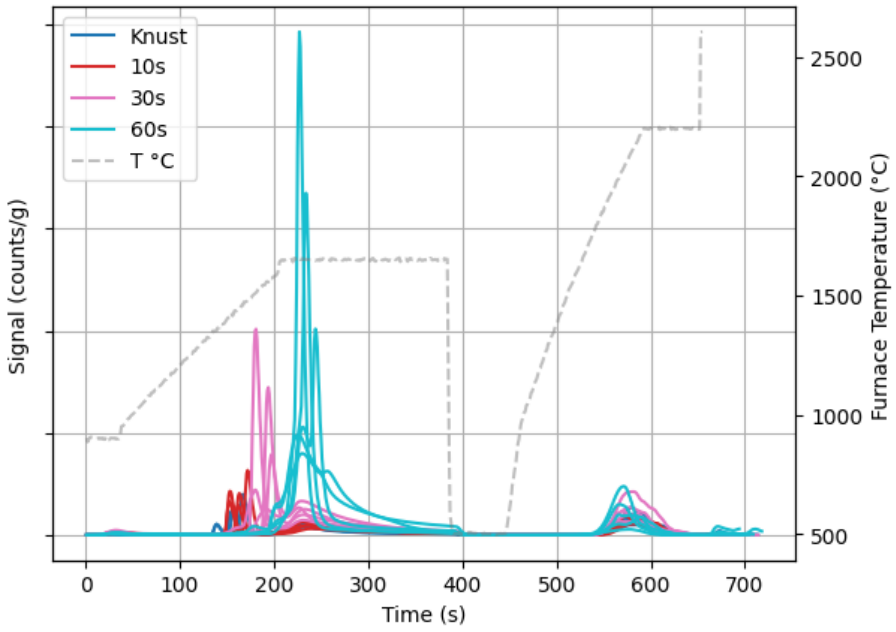


**Figure 6:** Oxygen signal profiles for MG-Si samples with varying milling durations

Quantitative analysis of peak areas supports these observations. In the $SiO_x$ integration region, the mean oxygen signal increases systematically with milling time, from 4601 counts · s · $g^{-1}$ for the as-received sample to 28419 count · s · $g^{-1}$ after 60 s of milling (Table II). The relative standard deviation (RSD) remains within acceptable limits (7.4 – 15.0 %), considering the inherent inhomogeneity of the material. Statistical analysis (t-tests) confirms that all pairwise differences are significant ($p < 0.001$).

**Table II:** Statistical measures of peak areas in the $SiO_x$ integration region

| | As received | 10 s | 30 s | 60 s |
|---|---|---|---|---|
| **SSA [$m^2 \cdot g^{-1}$]** | 0.20 | 0.51 | 1.96 | 3.17 |
| **Avg. Area [counts • s • $g^{-1}$]** | 4601 | 6282 | 15447 | 28419 |
| **STD [counts • s • $g^{-1}$]** | 513 | 467 | 2309 | 2853 |
| **RSD [%]** | 11.2 | 7.4 | 15.0 | 10.0 |

In contrast, the slag integration region shows no consistent trend with milling time (Table III). Although RSD values are higher (19.2 – 48.1 %), this is primarily due to lower signal magnitudes rather than increased variability, as indicated by comparable standard deviations. Statistical testing yields $p > 0.01$ for all comparisons, confirming that differences are not significant at the 99 % confidence level.

**Table III:** Statistical measures of peak areas in the slag integration region

| | As received | 10 s | 30 s | 60 s |
|---|---|---|---|---|
| **SSA [$m^2 \cdot g^{-1}$]** | 0.20 | 0.51 | 1.96 | 3.17 |
| **Avg. Area [counts$\cdot s \cdot g^{-1}$]** | 3654 | 3156 | 5515 | 4777 |
| **STD [counts$\cdot s \cdot g^{-1}$]** | 870 | 607 | 2462 | 2299 |
| **RSD [%]** | 23.8 | 19.2 | 44.6 | 48.1 |

These results indicate that the low-temperature signal is sensitive to surface oxide content, whereas the high-temperature signal is independent of particle size and can be attributed to slag.

Overall, the findings demonstrate that the temperature-ramped LECO method enables effective separation of oxygen contributions from surface oxides and slag. The systematic increase in the $SiO_x$ signal with milling, combined with the stability of the high-temperature signal, confirms the method's capability to distinguish between these two sources of oxygen.

## 4. CONCLUSIONS

For industrial silicon production, a reliable slag measurement system based on robust oxygen quantification is critical to ensure consistent quality control and minimise variability arising from sample preparation and measurement uncertainty. This work demonstrates that a temperature-ramped IGF method can significantly improve accuracy in the estimation of slag-bound oxygen in silicon materials. The incorporation of nickel as a selective flux enhances the decomposition of surface silicon oxides, reducing their contribution to the slag-related signal. The effectiveness of the method was confirmed through the milling experiment, which showed that variations in particle size — and thus surface area — affect only the $SiO_x$ signal, while the slag-related signal remains unchanged under selected analytical conditions. This indicates that the combined temperature ramping and nickel-assisted approach reduces the effect of samples particle size on slag-bound oxygen significantly.

Overall, the results establish a proof-of-concept for a temperature-programmed IGF analysis capable of selectively separating and quantifying oxygen contributions from surface oxides and slag. Therefore, the presented method provides a more representative assessment of slag content and has clear potential to improve analytical robustness and quality control in silicon production.

Future work will focus on the full industrial validation of a quantitative method for slag estimation, by verifying accuracy, precision, and reproducibility. The final step will be the transfer of the validated method to quality control laboratories at production sites.

Moreover, the validation of similar methods could be extended also to a broader range of industrial materials, particularly FeSi and FSM, as well as further optimisation of the temperature programme to reduce analysis time while maintaining signal separation.

## 5. ACKNOWLEDGEMENTS

This paper is published by permission of Elkem ASA. The contribution of our colleague Pål Baggethun is gratefully acknowledged. This work has been funded by Research Council of Norway (RCN) through SFI PhysMet – Centre for Sustainable and Competitive Metallurgical and Manufacturing Industry (Project number: 309584).

## 6. REFERENCES

Assael M.J., Chatzimichailidis A., Antoniadis K.D., Wakeham W.A., Huber M.L. and Fukuyama H. 2017. Reference correlations for the thermal conductivity of liquid copper, gallium, indium, iron, lead, nickel and tin. *High Temperature High Pressure*, Vol.46(6), pp.391-416. https://doi.org/10.3233/HTHP-170303.

Balakos M.W. and Chuang, S.S.C. 1993. CO disproportionation on Ni-based catalysts. *Reaction Kinetics and Catalysis Letters,* Vol.49, pp.7–12. https://doi.org/10.1007/BF02084022.

Beck H. and Müller H. 1997. Determination of the oxygen content of ceramic materials by Carrier-Gas-Heat-Extraction (CGHE) – feasibility and restrictions of the method. *Fresenius Journal of Analytical Chemistry.* Vol.357, pp.652–655. https://doi.org/10.1007/s002160050229.

Brunauer, S., Emmett, P. H. and Teller, E. 1938. Adsorption of gases in multimolecular layers. *Journal of the American Chemical Society*, 60(2), pp.309–319. https://doi.org/10.1021/ja01269a023.

Cao R., Li Y., Xia J., Chen Z. and Yang J. 2019. $NiSO_4$ as Additive Effect on the Carbothermal Reduction Process of Phosphate Rock and $SiO_2$. *Silicon,* Vol.11, ..2829–2836. https://doi.org/10.1007/s12633-019-0071-x

Chahtou A., Boucetta A., Benioub R., Boualem A., Hamzaoui S. and Itaka, K. 2020. Study of Carbothermal Reduction of Silica, Alumina and Titania Under Argon Gas. *Proceedings of the 1st International Conference on Renewable Energy and Energy Conversion 2019*. Oran, Algeria, 11-13 November 2019, pp.295-301. https://doi.org/10.1007/978-981-15-5444-5_37.

Chen C., Li W., Zhen Q., Li R., Zhang S., Li X. and Wang J. 2025. Controlled synthesis of silicon carbide whiskers via nickel-based alloy catalyst-assisted carbothermal reduction unraveling vapor-liquid-solid growth and $Ni_3Si_2$ droplet dynamics. *Ceramics International*, Vol. 51, Issue 19, pp.29770-29780. https://doi.org/10.1016/j.ceramint.2025.04.180.

Elkem ASA (2024). *Product Data Sheet: Metallurgical Silicon (MG-Si), Revision No. 01, 14 March 2024*. Elkem ASA, Oslo, Norway. Available at: Elkem Product Data Sheet MG-Si (Accessed: 23 July 2026).

Elkem ASA (n.d.) Elkem. Available at: https://www.elkem.com/ (Accessed: 13 May 2026).

Gruner W. and John A. Determination of oxygen in solids using a modified carrier gas-hot extraction method. 1992. *Fresenius Journal of Analytical Chemistry,* Vol.342, pp.51–53. https://doi.org/10.1007/BF00321689.

Forwald A.G., Rong H.M. and Vogelaar G.C. 1994. Oxygen in Silicon; occurrence and influence on the direct process to methylchlorosilane. *Proceedings of the Silicon for the Chemical and Solar Industry II*. Loen, Norway, 8-10 June 1994, pp.107-119.

Jiang Y., Lin X., Ideta K., Takebe H., Miyawaki J., Yoon S.H. and Mochida I. 2014. Microstructural transformations of two representative slags at high temperatures and effects on the viscosity. *Journal of Industrial and Engineering Chemistry*, Vol.20, Issue 4, pp.1338–1345. https://doi.org/10.1016/j.jiec.2013.07.015.

Johnston M.D. and Barati M. 2010. Distribution of impurity elements in slag–silicon equilibria for oxidative refining of metallurgical silicon for solar cell applications. *Solar Energy Materials and Solar Cells*, Vol.94, Issue 12, pp.2085-0290. https://doi.org/10.1016/j.solmat.2010.06.025.

Kim B.-C., Uono H., Fuse T., Ishihara T., Senna M. Fabrication of nano-sized Si powders with a narrow size distribution by two-step milling. 2011. *Journal of Materials Research*. Vol.18, Issue 6, pp.1368-1373. https://doi.org/10.1557/JMR.2003.0188.

Kuivila, C.S. and Miller, D.C. 1999. *Method for selecting chemical grade silicon metalloid having improved performance in a direct process for making diorganodihalosilanes*. United States Patent US 5,973,177, issued 26 October 1999.LECO Corporation (n.d.) 836 Series elemental analysis for oxygen, nitrogen and hydrogen detection. Available at: https://www.leco.com/products/836-series/ (Accessed: 13 May 2026).

Lee H.-C., Dhage S., Akhtar M. S., Kwak D.H., Lee W.J., Kim C.-Y., and Yang O-B. 2010. A simulation study on the direct carbothermal reduction of SiO2 for Si metal. *Current Applied Physics*, Vol.10, Issue 2, Supplement, pp.S218-S221. https://doi.org/10.1016/j.cap.2009.11.053.

L'vov, B.V. 2000. Mechanism of carbothermic reduction of iron, cobalt, nickel and copper oxides. *Thermochimica Acta*, 360, pp.109–120. https://doi.org/10.1016/S0040-6031(00)00540-2.

Maeng S.H., Lee H., Park M.S., Park S., Jeong J. and Kim S. 2020. Ultrafast carbothermal reduction of silica to silicon using a $CO_2$ laser beam. *Scientific Reports,* Vol.10, pp.21730. https://doi.org/10.1038/s41598-020-78562-1.

Maslennikova A.A., Tkacheva O.Y. and Zaikov Y.P. 2025. Carbothermic Reduction for the Quantitative Determination of the Oxygen Content in Various Materials (Review). *Russian Metallurgy*, Vol.2025, pp.1924–1931. https://doi.org/10.1134/S0036029525702957.

Nilssen B.E. and Kleiv R.A. 2020. Silicon powder properties produced in a planetary ball mill as a function of grinding time, grinding bead size and rotational speed. *Silicon*, Vol.12, pp.1–12. https://doi.org/10.1007/s12633-019-00340-0.

Næss M.K., Kero I., Tranell G., Tang K., and Tveit H. 2014. Element Distribution in Silicon Refining: Thermodynamic Model and Industrial Measurements. *JOM*, Vol.66, pp.2343-2354. https://doi.org/10.1007/s11837-013-0797-7.

Olivo A., Michels, L., Høyen M.M., Friestad K. and Di Sabatino, Marisa. 2024 Ageing of micro and nano silicon surface (May 15, 2024). *Proceedings of the Silicon for the Chemical and Solar Industry XVII*. Trondheim, Norway, 7-10 September 2024, pp.295-301. https://doi.org/10.1007/978-981-15-5444-5_37.
http://dx.doi.org/10.2139/ssrn.4941273

Ostrovski O., Zhang G., Kononov R. and Dewan M.A.R. 2010. Carbothermal solid state reduction of stable metal oxides. *Steel Research International*, Vol.81(10), pp. 841–846. https://doi.org/10.1002/srin.201000177.

Petrakis E. and Komnitsas K. 2022. Effect of grinding media size on ferronickel slag ball milling efficiency and energy requirements using kinetics and attainable region approaches. *Minerals*, Vol.12(2), pp.184. https://doi.org/10.3390/min12020184.

Schei A., Tuset J.K. and Tveit H. 1998. *Production of High Silicon Alloys*. 1st ed. Trondheim: Tapir Forlag. ISBN 8251913179

Shen T.D., Shmagin I., Koch C.C., Kolbas R.M., Fahmy Y., Bergman L., Nemanich R.J., McClure M.T., Sitar Z. and Quan M.X. 1997. Photoluminescence from mechanically milled Si and $SiO_2$ powders. *Physical Review B*, Vol.55(12), pp.7615–7623. https://doi.org/10.1103/PhysRevB.55.7615.

Skoog D.A., Holler F.J. and Crouch S.R. 2017. *Principles of Instrumental Analysis*. 7th ed. Boston: Cengage Learning. ISBN 9781305577213

Swamy V. and Dubrovinsky L.S. 1997. Thermodynamic data for the phases in the $CaSiO_3$ system. *Geochimica et Cosmochimica Acta*, Vol.61, Issue 6, pp.1181-1191. https://doi.org/10.1016/S0016-7037(96)00403-6.

Watanabe T. 2025. Kinetics of thermal oxidation of silicon. *Applied Physics Express*, Vol.18, 120101. https://doi.org/10.35848/1882-0786/ae1f5b.

**Sophia Anastasia Wellman**
*Technical Trainee, Elkem*

Sophia holds a Master of Science degree in Applied Physics and Mathematics from the Norwegian University of Science and Technology. During the summer of 2025, she worked as a summer student at Elkem Silicon Products Development in Kristiansand, where she carried out the work presented in this paper.

During the 2025/2026 academic year, she completed both her project work and master's thesis in collaboration with Elkem, focusing on the chemical characterization of oxide layers on silicon powders. In August 2026, she joined Elkem ASA as a Technical Trainee, continuing the research project initiated during her summer internship.